Modifications to the Rapid Update Cycle Land Surface Model (RUC LSM) available in the Weather Research and Forecast (WRF) model

Tatiana G. Smirnova[1,2], John M. Brown[1], Stanley G. Benjamin[1], Jaymes S. Kenyon[1,2]

[1] NOAA Earth System Research Laboratory (NOAA/ESRL)

[2] Cooperative Institute for Research in Environmental Sciences (CIRES)

Boulder, CO

Resubmitted for publication in *Monthly Weather Review*

30 November 2015

Original submission – May 2015

Second submission – 7 September 2015

Corresponding Author:

Tatiana G. Smirnova

Global Systems Division (GSD)

NOAA Earth System Research Laboratory (NOAA/ESRL)

325 Broadway, Boulder, CO, 80305

Email: Tanya.Smirnova@noaa.gov

Phone: (303)-497-6253

Fax: (303)-497-4176

Abstract

The land-surface model (LSM) described in this manuscript was originally developed as part of the NOAA Rapid Update Cycle (RUC) model development effort and, with ongoing modifications, is now used as an option for the WRF community model. The RUC model and its WRF-based NOAA successor, the Rapid Refresh (RAP), are hourly updated and have an emphasis on short-range, near-surface forecasts including aviation-impact variables and pre-convective environment. Therefore coupling to this LSM (hereafter, RUC LSM) has been critical to provide more accurate lower boundary conditions. This paper describes changes made to the RUC LSM since earlier descriptions, including extension from 6 to 9 levels, improved snow treatment, and new land-use data from MODIS.

The RUC LSM became operational at the NOAA National Centers for Environmental Prediction (NCEP) as part of the RUC from 1998–2012 and as part of the RAP from 2012 through present. The simple treatments of basic land-surface processes in the RUC LSM have proven to be physically robust and capable of realistically representing the evolution of soil moisture, soil temperature, and snow in cycled models. Extension of the RAP domain to encompass all of North America and adjacent high-latitude ocean areas, necessitated further development of the RUC LSM for application in the tundra permafrost regions and over Arctic sea ice. Other modifications include refinements in the snow model and a more accurate specification of albedo, roughness length and other surface properties. These recent modifications in RUC LSM are described and evaluated in this paper.

1. Introduction

The context of this work is an ongoing effort within the NOAA Earth System Research Laboratory to improve prediction of land-surface and hydrological properties in NOAA models. The land-surface model (LSM) described in this paper was originally developed to provide more accurate lower boundary conditions for the hourly updated NOAA Rapid Update Cycle (RUC) model focusing on short-range aviation and severe weather prediction (Benjamin et al. 2004a) but has now been extended to wider geographical application. These recent applications include the Weather Research and Forecast (WRF) model (Skamarock et al. 2008) and the NOAA hourly updated Rapid Refresh (RAP, Benjamin et al. 2015) and High-Resolution Rapid Refresh (HRRR, Smith et al. 2008) models. The goal of this study is to describe and validate the modifications to RUC LSM that are motivated by these new applications.

A previous six-level version of a land-surface soil/vegetation scheme (Smirnova *et al.,* 1997) was incorporated into the cycled RUC model to improve its predictions of surface fluxes and atmospheric boundary-layer properties by explicitly predicting soil moisture and temperature and full soil condition cycling dependent on short-range prediction and frequent data assimilation. This provided an alternative to use of climatological soil values that can result in significant errors during and after dry or rainy periods. Later, this surface model, referred to as the RUC LSM, was enhanced to include a snow model and frozen soil processes (Smirnova *et al.,* 2000). The parameterizations in the RUC LSM describe complicated atmosphere/land surface interactions in an intentionally simplified fashion to avoid excessive sensitivity to multiple uncertain surface parameters. Nevertheless, the RUC LSM, when coupled

with the hourly-assimilating RUC atmospheric model, demonstrated over years of ongoing cycling (Benjamin et al 2004a,b, Berbery et al., 1999) that it can produce a realistic evolution of hydrologic and time-varying soil fields (i.e., soil moisture and temperature) that cannot be directly observed over large areas. This result is possible only if the soil/vegetation/snow component of the coupled model, constrained only by atmospheric boundary conditions and the specification of surface characteristics, has sufficient skill to avoid long-term drift.

In order to validate physical parameterizations, land-surface models are customarily tested off-line and forced with observed atmospheric conditions, thereby providing a controlled environment so model behavior can be assessed. A set of more recent RUC LSM modifications (Table 1) have been developed and evaluated through such off-line testing and coupled numerical weather prediction (NWP) testing, as described in this paper. International projects for intercomparison of land-surface and snow parameterization schemes were essential in providing this testing environment and afforded an excellent opportunity to evaluate the RUC LSM with different land use and soil types and within a variety of climates. The RUC LSM was included in Phase 2-d of the Project for the Intercomparison of Land-Surface Prediction Schemes (PILPS-2d), in which tested models performed 18-year simulations of the land-surface state (Schlosser *et al.,*1997, Slater *et al*., 2001, Luo *et al*., 2003). The RUC LSM was also tested during the Snow Models Intercomparison Project (SnowMIP and SnowMIP2), with emphasis on snow parameterizations for both grassland and forest locations (Etchevers et al, 2002, 2004; Essery et al. 2009; Rutter et al. 2009). Selected results from these off-line experiments will be presented in this paper.

In 1998, the initial RUC LSM was implemented in the operational RUC at NCEP, then became available worldwide in 2002 as an LSM option through the WRF community model (http://wrf-model.org; Skamarock *et al.*, 2008). The RAP model (Benjamin *et al.,* 2007, 2015), implemented at NCEP in May 2012 (and replacing the RUC), uses the Advanced Research WRF (ARW) dynamical core as the prognostic atmospheric model component and the RUC LSM option as its land-surface component. With the RAP domain extending into the Arctic region (Fig. 1), the RUC LSM needed further development to improve an interactive coupling of the atmosphere with the underlying surface where it is ice-covered.

As a first step, a simple sea-ice treatment and further snow component enhancements were added to the RUC LSM. Later, vertical resolution in the soil domain was increased to have nine levels instead of six to improve the diurnal cycle near the surface. These enhancements to RUC LSM (Table 1), along with test results from stand-alone, one-dimensional experiments, and within the coupled RAP framework, are described in Section 2. All of these enhancements are available in WRF using the RUC LSM option. Section 3 describes the new Moderate-Resolution Imaging Spectroradiometer (MODIS)-derived classification of land-surface properties available in WRF and used in the RAP and HRRR, providing more up-to-date land surface cover over its predecessor, the USGS land-use classification scheme used in the RUC. The improved RUC LSM also utilizes higher resolution MODIS Fractional Photosynthetically Active Radiation (FPAR) and Leaf Area Index (LAI) datasets to specify vegetation fraction and leaf area index (applied in RAP and HRRR). Section 3 also describes the new capability of the RUC LSM to specify land-surface parameters as area-weighted averages in the grid box. Concluding remarks are presented in Section 4.

2. Description of sea-ice parameterization and modifications to the snow model

The RUC LSM contains heat and moisture transfer equations, together with energy and moisture budget equations for the ground surface, and uses an implicit scheme for computing the surface fluxes (Smirnova *et al.,* 1997). The energy and moisture budgets are applied to a thin layer spanning the ground surface and consider the heat capacities and densities of both the soil/snow and the atmosphere. The version of this model, tested in 1-D off-line tests and implemented in the first version of the RAP model, had six prognostic soil levels, ranging from the soil surface to 300 cm in depth (0, 5, 20, 40, 160, 300 cm). The version in the WRF repository (version 3.4.1 since 2012, Table 1) used in the operational RAPv2 (Benjamin et al 2015) uses nine prognostic soil levels (0, 1, 4, 10, 30, 60, 100, 160, 300 cm), with highest vertical resolution near the surface (top layer of 1 cm). The thinner top soil layer with 9 levels provides a stronger diurnal cycle as shown in a parallel RAP experiment (Fig. 2). The smaller cold bias in daytime and warm bias at nighttime results from use of the 9-level LSM compared to that with the 6-level LSM. The RUC LSM has a snow model with one or two additional snow levels depending on snow depth and a simple parameterization of the processes in frozen soil (Smirnova *et al*., 2000). Recent enhancements to the RUC LSM in all of these areas are addressed below and summarized in Table 1.

a. Parameterization of processes in sea ice

Treatment of processes in sea ice has been added to the RUC LSM parameterizations. This was deemed necessary due to RAP domain coverage in high-latitude ocean areas. The ice model accounts for thermodynamic processes by solving the vertical heat diffusion equation:

$$\frac{\partial T_i}{\partial t} = \frac{\partial}{\partial z}\left(\frac{\nu_i}{\rho_i c_i}\frac{\partial T_i}{\partial z}\right), \quad (1)$$

where T_i is the temperature, and ν_i, c_i and ρ_i are sea-ice thermal conductivity, specific heat capacity, and density, respectively (a list of symbols is provided in the Appendix). Sea-ice properties are assumed to be those of pure ice. To limit computational expense for short-range weather-prediction applications, the adjustment for ice salinity is disregarded for now. This parameterization is applied equally to sea ice and lake ice. The specific heat capacity for pure ice is computed from an empirical formula for temperatures from −2 to –40°C (Zubov, 1979):

$$\boldsymbol{c_i = 0.5057 + 0.001863\, T_i}, \quad (2)$$

where T_i is the temperature (°C). The coefficient of thermal conductivity of pure ice devoid of air bubbles is set to

$$\nu_i = 2.260872\ J(m\ s\ K)^{-1}, \quad (3)$$

based on an average of published values. The density of pure ice is given by

$$\rho_i = \frac{\rho_0}{1+0.000165\, T_i}, \quad (4)$$

where ρ_0 is pure ice density at 0°C (917.6 kg m^{-3}).

The energy budget at the sea ice surface is written as:

$$\left(\rho_a c_p\, \Delta\, z_a + \rho_i c_i\, \Delta\, z_i\right)\frac{\partial\, T_{sk}}{\partial t} = \{R_n - H - L_s E - M_i\}|_{\Delta z_a} - G_i\,|_{\Delta z_i}, \quad (5)$$

where $\Delta\, z_a$ is the height of the middle of the first atmospheric layer, $\Delta\, z_i$ is the depth of the middle of the top layer of sea ice, T_{sk} is the mean temperature of a thin layer spanning the

atmosphere–ice interface, R_n is the net radiative flux into the surface layer, *H* is the sensible heat flux into the atmosphere, L_s is the latent heat of sublimation, *E* is the sublimation rate, and G_i is the heat flux into the sea ice. With T_{sk} constrained to stay below the sea-ice freezing point, the energy budget may produce a positive residual M_i that could be used to melt sea ice. However, currently the RUC LSM does not provide treatment of melted sea ice. Sea-ice coverage in RAP is updated daily from the operational IMS (Interactive Multisensor Snow and Ice Mapping System) Northern Hemisphere Snow and Ice Analysis at 4-km resolution (Helfrich *et al.*, 2007).

When snow falls on a sea-ice surface, a two-layer snow model is applied to the snow accumulated on sea ice in a manner similar to snow accumulation on land (Smirnova *et al*., 2000). In this case, the energy-budget equation is applied to the atmosphere–snow interface:

$$\left(\rho_a c_p \,\Delta\, z_a + \rho_{sn} c_{sn} \,\Delta\, z_{sn}\right) \frac{\partial\, T_{sk}}{\partial t} = \{R_n - H - L_s E - M_{sn}\}|_{\Delta z_a} - G_{sn}\,|_{\Delta z_{sn}}\,, \quad (6)$$

where M_{sn} is an energy-budget residual when snow-surface temperature is constrained not to exceed the freezing point, and this residual energy is used to melt snow. Application of the snow model in areas covered with sea ice has been found to be helpful in producing realistic surface conditions, aided further by the hourly cycling of snow depths and snow temperatures in the RAP. This cycling of LSM conditions, including snow, allows the RAP (or HRRR) to maintain physically realistic vertical air-surface temperature differences (either positive or negative or near zero) at each grid point. In the simplified approach previously used in RUC LSM, snow did not accumulate on the sea-ice surface and sea-ice skin temperature was equated to that at the first atmospheric level. Now, the solution of the energy budget in (6) takes into account the insolating effects of the snow cover and may produce warmer skin

174 temperatures in snow covered sea-ice regions during the daytime. This is demonstrated in a
175 case study comparison (Fig. 3a, off the northern coast of Alaska), and also in warmer surface-
176 layer temperatures from the positive upward sensible heat fluxes (Fig. 3b). The case study
177 presented in Fig. 3 demonstrates that during the day, positive downward heat fluxes from the
178 surface of sea ice into its deeper layers (Fig. 3c) store heat inside sea ice, precluding the
179 unrealistically cold nighttime 2-m temperatures resulting from the previous approach in this
180 case.

181 This more sophisticated sea-ice treatment has been important for arctic applications in
182 the WRF Rapid Refresh. For example, weather predictions over land in such regions as Alaska
183 can be significantly improved from more realistic surface conditions, where nearby sea ice may
184 be present in adjacent waters for much of the year. Figure 4a presents an example of a
185 common synoptic situation for the Alaska region, where onshore winds bring air inland from
186 the nearby ice-covered Bristol Bay. With the previous approach without RAP-cycled snow
187 temperatures on sea ice, unrealistically cold temperatures over sea ice led to significant 2-m
188 cold biases over inland regions of Alaska (circled region, Fig. 4b). With the new treatment of
189 snow on sea ice in the RUC LSM, warmer near-surface layers over sea ice were produced and
190 transported inland, significantly reducing RAP inland cold biases in southwestern Alaska for this
191 case (circled region, Fig. 4c).

192

193 **b. Modifications to the RUC LSM snow model**

194 **1) Snow melting algorithm**

Previous monitoring of RUC LSM behavior during the cold season revealed weaknesses in its snow model. Excessive snow melting rates associated with warm advection over snow was one such deficiency. During these events, sensible heat fluxes from the warm atmosphere towards the cold snow surface could become very large. As a result, energy budget residuals (Eq. 6, term M_{sn}) used for snow melt could also become very large, causing large amounts of snowmelt during a single time step. However, field experiments have demonstrated that melting rates are physically limited and depend on vertical temperature gradients just above the surface (Eggleston *et al*., 1971). When energy residuals from the model energy budget solution exceed a maximum threshold for realistic snow melt, the excess energy can be assumed to warm the air nearest the snow surface. As a result, skin temperatures can rise to above freezing, even with snow on the ground. The 2-m air temperature can also warm, but with a corresponding reduction in snow melting rates and an overall prolonged presence of snowpack.

This strategy of limiting melting rates has now been implemented in the RUC LSM via a two-iteration solution of the energy budget (Eq. 6). At the first iteration, the skin temperature is limited to 273.15 K (with the full snow coverage of the grid cell), and the residual energy (Eq. 6, term M_{sn}) is computed. After constraints on melting rates for given conditions (Eggleston *et al*., 1971) are applied, an updated maximum possible energy for snow melt is determined. If this updated M_{sn} is less than that from the first iteration, the updated M_{sn} is retained in the overall solution, providing more realistic (slower) snow melting rates and warmer (above-freezing) skin temperatures.

Off-line testing of modified snow melt physics in the RUC LSM using SnowMIP2 data over multiple years and for different locations confirmed that the two-iteration algorithm helps to produce more realistic snow melting rates in spring season. The new algorithm was also tested in the coupled model (RAP) in winter for a 10-day long period from 1-10 January 2015. This period featured several snow storms passing through the US southern plains, the Midwest and North Atlantic states. One particular snow storm over Arizona, New Mexico and Texas on 2-3 January 2015 with rapid snowmelt expedited by warm advection from close-by snow-free areas, provided a good case to see the benefits from changes to the snow melting algorithm. As anticipated, the control run with the old approach was melting snow too fast, causing underestimation of its snow cover on the next day after the passage of the snowstorm. Deficient snow cover in the control run on 4 January 2015 contributed towards its larger warm biases (Fig. 5a) and higher 2-m temperature RMS errors (Fig. 5b) averaged over all CONUS domain compared to the test run with the new two-iteration algorithm. Other days of the 10-day period featured slow melting processes and did not show any significant differences between the two runs. Also, excessive melting in the control run was mitigated by using IMS snow/sea-ice data (Helfrich *et al.*, 2007) to update the horizontal snow coverage once daily.

The snow updating procedure (Benjamin et al 2015, Section 4) conducted once daily at 0000 UTC includes trimming of horizontal model snow coverage if there is no snow in the IMS snow/sea-ice data for the given grid point and only if there is no snow precipitation in the model. The algorithm keeps track of trimmed snow water equivalent and adds it to existing neighboring points with missing snow compensating for possible shifts in model snow precipitation placement. For grid points with missing snow that do not have neighbors with

trimmed snow, the value of built snow water equivalent is computed as an average from the neighboring snow points or, in case this is a stand-alone grid point with missing snow, is set to a minimum value of 1 kg m^{-2}. A similar procedure is used to decrease skin and soil temperatures (3 levels in soil with a 6-level and 5 levels with a 9-level configuration) if they exceed 273 K for the points with built snow.

While both runs applied the daily snow updating procedure, the control run received larger benefits from the snow-building component that helped to correct significant underestimation of cycled snow in this run. When the snow-updating procedure was applied on 4 January at 0000 UTC, the number of points with built snow was 26% higher in the control run, and the overall number of grid points with corrected snow cover was 8% higher. This indicates that the two-iteration snow melting algorithm produced more realistic melting rates and more accurate snow cover on the ground. Both RAP runs (Fig. 6a,b) were compared to the NOHRSC (National Operational Hydrologic Remote Sensing Center) daily snow analyses valid at 0600 UTC (Fig. 6c). This comparison shows that even after snow updating, the control run still has underestimated snow-water equivalent values and less accurate location of the snow band across Arizona, New Mexico and Texas (Fig. 6a, see area inside the red oval) than the experimental run (Fig. 6b). In the next snow update on 5 January 2015, the number of points with built snow in the control run was 33% higher, meaning that excessive melting rates in this run persisted. This example illustrates that both snow updating from the IMS snow product and improvements in the snow melting algorithm contribute to a correct coverage of cycled snow in RAP.

2) Snow albedo

Further efforts were undertaken to achieve a more accurate representation of snow surface properties, such as albedo, that strongly influence the energy budget. As a first step, a climatological, areally-weighted, clear-sky maximum surface albedo in snow-covered areas, computed from Defense Meteorological Satellite Program (DMSP) imagery brightness in 1° latitude–longtitude cells (Robinson and Kukla, 1985), has been included in the RAP version of the RUC LSM. This dataset, available in WRF, depicts highest values of surface albedo (~0.80) in snow-covered high-latitude tundra and open shrubland regions, minimum values (~0.35) within the 56–60°N zonal region, where snow albedo is affected by the prevalent boreal forest cover, and more typical values for snow albedo (~0.70) over the US Great Plains, where crop and grassland vegetation types are dominant (Fig. 7). These values of surface albedo are interpolated to the RAP grid, and provide vegetation dependent spatial variability in the surface albedo in areas of snow cover instead of the constant value of snow albedo (0.75) used previously.

Several modeling studies have found that use of this dataset can have a large impact on the surface energy budget and near-surface temperatures (e.g., Viterbo and Betts, 1999), affecting the timing of spring snowmelt and subsequent streamflow peaks (Thomas and Rowntree, 1992). Similar impacts were monitored in the RAP application, especially pronounced in snow-covered forested regions of Canada, Alaska and the eastern part of the continental US domain with lower values of maximum surface albedo (Fig. 7).

The RAP control simulation with constant value of fresh snow albedo equal to 0.75 and experimental simulation with the use of this maximum surface albedo dataset were performed

for the same 10-day period in January 2015 as described in Section 2.b.1. During and after passages of several snowstorms, more accurate specification of surface albedo in the experimental configuration showed improved performance near the surface. In particular, daytime cold biases in 6-h forecasts of 2-m temperature averaged over the eastern US region were smaller in the experimental simulation due to increased amount of solar energy absorbed by the surface layer (Fig. 8a). Also, average 2-m temperature STD errors were reduced during the day, while at night, when surface albedo has no influence on model performance, errors remain at the same level (Fig. 8b). Figure 8 demonstrates that daytime improvements in surface temperature predictions from better representation of surface albedo, and consequently a more accurate surface energy budget, can be substantial. Therefore, to further improve near-surface predictions in snow-covered regions of RAP and HRRR, our future plans include testing a recently developed higher resolution 0.05-degree dataset of maximum surface albedo of the snow-covered land generated from several MODIS sensors (Barlage *et al.*, 2005).

In addition to its dependence on vegetation type, snow albedo in the RUC LSM (as implemented in RAP) varies as a function of snow age, snow depth, and also snow temperature (when it approaches the melting point of 0°C). The temperature dependence of snow albedo is such that higher temperatures lower the albedo due to meltwater pockets on the surface and changes to the ice crystal structure (Robock 1980; Petzold 1977). Following Robock (1980), snow and ice albedos are assumed to vary linearily from a maximum surface value for a snow-covered area at $T \leq -10$°C to a "meltwater" value at $T \geq 0$° C, where "meltwater" value equals 0.4 for flat surfaces (cropland, grassland, sea ice, etc.) and 0.3 for forests.

303 The temperature dependence of RUC LSM snow albedo was tested off-line using
304 observed atmospheric conditions from SnowMIP2 over multiple years and for several grassland
305 and forest locations in Canada, United States and Europe (Essery et al. 2009; Rutter et al. 2009).
306 Figure 9a (http://xweb.geos.ed.ac.uk/~ressery/SnowMIP2/results.html) shows, as an example,
307 snow-water equivalent simulations at a grassland location in the Swiss Alps from all LSMs
308 participating in SnowMIP2 for the 2003–2004 winter season. The spread among the models is
309 substantial, especially during the snow melting season. Many models melted snow too rapidly,
310 while others were too slow, including the RUC LSM. The stand-alone result from the RUC LSM
311 for the same location demonstrates that the RUC LSM captures well the observed variations of
312 snow cover on the ground during the first half of the winter season (Fig. 9b, red curve). But in
313 spring, RUC LSM is among the models that maintain snowpack for too long. The constant snow
314 albedo (0.75) previously used in the RUC LSM is the primary reason for this snowpack
315 maintenance, a value too high for the spring melting season. Implementing the albedo
316 temperature dependence described previously has helped to achieve a more realistic solution
317 of surface energy budget during the springtime, while not degrading model performance at
318 other times (Fig. 9b, green curve).
319 After extensive off-line testing in SnowMIP2, this snow albedo refinement was
320 implemented in the coupled Rapid Refresh. An example for a spring day with active snow
321 melting in the Arctic (Fig. 10) shows that with this new approach, the portion of the domain
322 covered by snow or ice exhibits albedos ranging from 0.5 to 0.8 (Fig. 10b), compared to the
323 constant albedo values of 0.55 for sea ice and 0.75 for snow (Fig. 10a) with the old approach.
324 Based on off-line testing, reduced albedos near the melting point can also produce more

realistic snow melting rates in the coupled RAP. The pattern of spatial variability also varies with time following the diurnal cycle of snow/sea-ice temperature. Together with the new treatment of sea ice and snow cover/temperature cycling in RAP (see Section 2.a, above), spatial and temporal variabilities of snow albedo in the Arctic have the potential to improve estimated net radiation and available melting energy for better prediction of surface conditions in this area.

3. Switch to MODIS land-use classification and FPAR/LAI data to specify surface parameters in Rapid Refresh.

Surface parameters such as aerodynamic roughness length, leaf area index, and emissivity are specified based on the dominant vegetation category for the model grid box, as gridded by the WRF Pre-processing System (WPS). WPS extracts the dominant land-use category and fractional land use data on specific model grids from a global dataset with 30" horizontal resolution. By default, the WPS program uses AVHRR-based USGS data, and these data were also utilized during the early stages of RAP model development and in the first verion of the operational RAP at NCEP. However, later an alternative dataset was added to WPS options, based on the MODIS land-cover classification of the International Geosphere-Biosphere Programme, and modified for the Noah land-surface model (Wang et al., 2014). Several studies have demostrated improved spatial and spectral characteristics in the MODIS data compared to older AVHRR data (Hansen et al., 2000, 2002a, 2002b). This suggests that the MODIS-derived vegetation maps more accurately represent the global land-cover distribution, and could be well suited for use in RAP.

346 The MODIS-based dataset contains 20 categories of land use (Fig. 12), that are not a
347 subset of the 24 USGS categories (Fig. 11). Therefore, additional tables specifying surface
348 parameters for the MODIS classification were provided for the RUC LSM starting with version
349 3.3 (released in 2011) of the WRF model. In addition to the new MODIS land use classification,
350 alternative datasets were added to WPS to specify vegetation fraction and leaf area index from
351 1-km resolution MODIS Fractional Photosynthetically Active Radiation (FPAR) and Leaf Area
352 Index (LAI) datasets (Tian et al., 2000). These new datasets were also introduced into the
353 second operational version of RAP.

354 Differences between the two classifications in several regions of the RAP domain can
355 lead to substantial differences in such important land-surface parameters as roughness length
356 (Fig. 13a). For example, inland from the western coast of Hudson Bay use of open shrubland in
357 MODIS (Fig. 12) instead of mixed forest in USGS (Fig. 11) reduces the roughness length by as
358 much as 0.6 m (Fig. 13a). Similarly, use of the cropland category in MODIS (Fig. 12) instead of
359 the cropland/woodland mosaic in USGS (Fig. 11) for the Midwestern United States reduces
360 roughness length by 0.132 m (Fig. 13a). Other regions of the RAP domain may have slightly
361 higher or even slighly lower values of roughness length with the MODIS classification. Changes
362 in this parameter certainly affect local wind speeds in the surface layer and the overall structure
363 of the boundary layer. However, the overall statistical verification of surface variables for the
364 RAP model has not been strongly affected by the transition to the MODIS land-use
365 classification, implemented in RAPv2 (Benjamin et al. 2015).

366 A pronounced improvement in RAP low-level wind forecast skill was achieved by
367 considering vegetation-based, subgrid heterogeneity (Fig. 14). This method subdivides the

surface within a RAP model grid box into several categories using MODIS or USGS land-use information. The effective values of surface parameters are then computed as weighted averages of parameters from each of the represented categories. With this approach, surface characteristics exhibit smoother transitions between grid points with different dominant land-use categories, and also reflect local variabilities within the grid cell. Including subgrid heterogeneity also tends to reduce differences in surface roughness between the USGS and MODIS classifications (Fig. 13b), such that the switch to the MODIS classification appears to have less impact on surface predictions.

The capability of representing subgrid heterogeneity in RUC LSM was tested over 10-day period in May 2013 in comparison to the control run of the model that used the dominant land-use category in each grid cell (Fig. 14). Both control and test configurations used WRF version 3.6 with the same suite of physics options including MYNN surface and boundary layer schemes. The test version showed consistent improvement over the control configuration in the 12-hour forecasts of 10-m wind for CONUS (Fig. 14), with mean positive wind speed biases reduction of about 0.02 m s^{-1} at night up to 0.1 m s^{-1} in daytime. Positive impact from including subgrid heterogeneity on surface wind predictions justified using this capability in the operational configuration of the RAP model.

4. Conclusions

Enhancements to the RUC LSM since 2000, partly motivated by NOAA's transition from the RUC model to the larger-domain RAP model, are summarized in Table 1. These enhancements focus on treatment for snow over land and ice and on the use of high-resolution

390 MODIS land-use parameters. They have been tested within a stand-alone, one-dimensional
391 framework and also coupled within the hourly-cycled RAP model, with improvement evident
392 from individual components including in the Arctic region. Nevertheless, real-time RAP forecast
393 performance metrics provide evidence that some RUC LSM parameterizations warrant further
394 improvement. For example, the second version of the operational RAP (RAPv2) has revealed
395 daytime warm/dry near-surface biases during the 2014 summer season, and cold 2-m
396 temperature biases over snow during the 2014-2015 cold season. Subsequent modifications in
397 the RAP model physics suite, including RUC LSM, will become a part of the third version of
398 operational RAP (RAPv3) at NCEP in early 2016 (Benjamin et al 2015).

399 Several very recent RUC LSM changes (not presented here) have been found to reduce
400 the warm/dry bias in lower-tropospheric, daytime, warm-season RAP forecasts over land. These
401 RUC LSM modifications are slated for inclusion in the next upgrade of the operational RAP. The
402 modifications include tuning of several soil parameters to increase evapotranspiration, along
403 with a simple representation of irrigation within cropland regions during the growing season.
404 Including a seasonally-varying roughness length over cropland, and MODIS based leaf area
405 index (LAI) climatology within deciduous vegetation, has also contributed to improved RAP
406 performance during the warm season.

407 In the cold season, further RUC LSM improvements could be achieved through
408 implementing the mosaic approach for grid cells partially covered with snow. In this approach,
409 the surface-energy budget of the snow-covered and non-snow-covered portions of a grid cell
410 are considered independently, then these independently determined surface fluxes are
411 aggregated to feed back into the surface-layer scheme. The benefits of the new approach will

412 be assessed from the traditional methods of LSM evaluation referred to in the introduction and
413 also from recently developed techniques for benchmarking intercomparisons (Best et al., 2015).
414 These very recent RUC LSM capabilities, along with the modifications detailed in this
415 paper, have been made available in the version 3.7 (2015) release of the WRF model. Further
416 work is in progress to make the RUC LSM available in the Land Information System (LIS)
417 developed at NASA (Kumar *et al.*, 2006). These recent (and continuing) improvements to the
418 RUC land-surface model improve its suitability for use within the WRF user community and for
419 potential global applications. Inclusion of the RUC LSM within LIS will allow contributions to LIS
420 applications within NASA and NOAA.
421
422 **Acknowledgments**
423

424 The work was supported by NOAA/ESRL and the Federal Aviation Administration (FAA)
425 Weather Research Program. We thank John Osborn of NOAA/ESRL and two anonymous
426 reviewers for thoughtful and very helpful reviews of the manuscript.

Appendix: List of Symbols

c_i - sea ice specific heat capacity, J/K;

c_{sn} - snow specific heat capacity, J/K;

c_p - air specific heat capacity;

E - sublimation rate, kg/m^2/s;

G_i - heat flux into sea ice, W/m^2;

G_{sn} - heat flux into snow, W/m^2;

H - sensible heat flux, W/m^2;

L_s - latent heat of sublimation, J/kg;

M_i - energy budget residual spent on sea ice melt, W/m^2;

M_{sn} - energy budget residual spent on snow melt, W/m^2;

R_n - net radiation flux, W/m^2;

T_i - ice temperature, K

T_{sk} - temperature of atmosphere/surface interface, K;

ν_i - sea ice thermal conductivity, W/m/K ;

ρ_a - air density, kg/m^3;

ρ_{sn} - snow density, kg/m^3;

ρ_i - sea ice density, kg/m^3;

ρ_0 - sea ice density at 0° C, kg/m^3;

Δz_a - depth of atmospheric surface layer, m;

Δz_i - depth of ice surface layer, m;

449 $\Delta\ z_{sn}$ - depth of snow surface layer.

References

Barlage, M., X. Zeng, H. Wei, and K. E. Mitchell, 2005: A global 0.05° maximum albedo dataset of snow-covered land based on MODIS observations, *Geophys. Res. Lett.*, **32**, L17405, doi:10.1029/2005GL022881.

Benjamin, S.G., D. Dévényi, S.S. Weygandt, K.J. Brundage, J.M. Brown, G.A. Grell, D. Kim, B.E. Schwartz, T.G. Smirnova, T.L. Smith, and G.S. Manikin, 2004a: An hourly assimilation/forecast cycle: The RUC. *Mon. Wea. Rev.*, **132**, 495-518, http://dx.doi.org/10.1175/1520-0493(2004)132<0495:AHACTR>2.0.CO;2.

Benjamin, S.G., G.A. Grell, J.M. Brown, T.G. Smirnova, and R. Bleck, 2004b: Mesoscale weather prediction with the RUC hybrid isentropic/terrain-following coordinate model. *Mon. Wea. Rev.*, **132**, 473-494, http://dx.doi.org/10.1175/15200493(2004)132<0473:MWPWTR>2.0.CO;2.

Benjamin, S. G., S. S. Weygandt, J. M. Brown, T. G. Smirnova, D. Devenyi, K. Brundage, G. A. Grell, S. E. Peckham, T. Schlatter, T. L. Smith, G. Manikin, 2007: From the radar-enhanced RUC to the WRF-based Rapid Refresh, *Preprints, 22nd Conf. Wea. Analysis Forecasting/18th Conf. Num. Wea. Pred.*, Park City, UT, Amer. Meteor. Soc., https://ams.confex.com/ams/22WAF18NWP/techprogram/paper_124827.htm.

Benjamin, S.G., S.S. Weygandt, M. Hu, C. Alexander, T. G. Smirnova, J.B. Olson, J.M. Brown, E James, D.C. Dowell, G.A. Grell, H. Lin, S. E. Peckham, T.L. Smith, W. R. Moninger, G.S. Manikin, 2015: A North American Hourly Assimilation and Model Forecast Cycle: The Rapid Refresh, *Mon. Wea. Rev.*, accepted for publication with revisions.

Berbery, E.H., K. Mitchell, S. Benjamin, T. Smirnova, H. Ritchie, R. Hogue, and E. Radeva, 1999: Assessment of land-surface energy budgets from regional and global models. *J. Geophys. Res*., **104**, 19329-19348. http://dx.doi.org/10.1029/1999JD900128

Best, M.J., G. Abramowitz, H. R. Johnson, A. J. Pitman, G. Balsamo, A. Boone, M. Cuntz, B. Decharme, P. A. Dirmeyer, J. Dong, M. Ek, Z. Guo, V. Haverd, B. J. J. van den Hurk, G. S. Nearing, B. Pak, C. Peters-Lidard, J. A. Santanello Jr., L. Stevens, N. Vuichard, 2015: The Plumbing of Land Surface Models: Benchmarking Model Performance, *J. Hydrometeorology*, **16**, pp.1425-1442, doi: http://dx.doi.org/10.1175/JHM-D-14-0158.1

Eggleston, Keith O., Israelsen, Eugene K., and Riley, J. Paul, 1971: Hybrid Computer Simulation of the Accumulation and Melt Processes in a Snowpack. *Reports.* Paper 501*,* http://digitalcommons.usu.edu/water_rep/501.

Essery, RLH, N Rutter, J Pomeroy, R Baxter, M Staehli, D Gustafsson, A Barr, P Bartlett and K Elder, 2009: SnowMIP2: An evaluation of forest snow process simulations. *Bull. Amer. Meteor. Soc.*, **90**, 1120-1135, doi:10.1175/2009BAMS2629.1.

Etchevers P., Martin E., Brown R., Fierz C. Lejeune Y., Bazile E., Boone A., Dai Y-J, Essery R., Fernandez A., Gusev Y., Jordan R., Koren V., Kowalczyck E., Nasonova R., Pyles D., Schlosser A., B.Shmakin A., Smirnova T. G., Strasser U., Verseghy D., Yamazaki T., Yang Z.-L., SnowMiP, 2002: An intercomparison of snow models: first results. *Proceedings of the International Snow Science Workshop*, Penticton, Canada, 29 Sep-4 Oct 2002, 8 p., http://arc.lib.montana.edu/snow-science/objects/issw-2002-353-360.pdf.

Etchevers P., Martin E., Brown R., Fierz C. Lejeune Y., Bazile E., Boone A., Dai Y-J, Essery R., Fernandez A., ev Y., Jordan R., Koren V., Kowalczyck E., Nasonova R., Pyles D., Schlosser A., B.Shmakin A., Smirnova T. G., Strasser U., Verseghy D., Yamazaki T., Yang Z.-L., 2004: Validation of the surface energy budget simulated by several snow models. *Annals of Glaciology*, **38**, 150-158, http://dx.doi.org/10.3189/172756404781814825.

Hansen, M. C., R. S. DeFries, J. R. G. Townshend, and R. Sohlberg, 2000: Global land cover classification at 1km spatial resolution using a classification tree approach. *Int. J. Remote Sens*., **21**, 1331–1364, doi:10.1080/014311600210209.

Hansen, M. C., R. S. DeFries, J. R. G. Townshend, L. Marufu, and R. Sohlberg, 2002a: Development of a MODIS tree cover validation data set for Western Province, Zambia. *Remote Sening of Environment,* **83**, 320–335, http://dx.doi.org/10.1016/S0034-4257(02)00080-9.

Hansen, M. C., DeFries, R. S., Townshend, J. R. G., Sohlberg, R. A., Dimiceli, C., and Carroll, M., 2002b: Towards an operational MODIS continuous field of percent tree cover algorithm: Examples using AVHRR and MODIS data, *Remote Sensing of Environment*, **83**, 303-319, http://dx.doi.org/10.1016/S0034-4257(02)00079-2.

Helfrich, S. R., D. McNamara, B. H. Ramsay, T. Baldwin, and T. Kasheta. 2007: Enhancements to, and forthcoming developments to the Interactive Multisensor Snow and Ice Mapping System (IMS), *Hydrological Processes,* **21**, 12, 1576-1586, doi: 10.1002/hyp.6720.

Kumar, S.V., C.D. Peters-Lidard, Y. Tian, P.R. Houser, J. Geiger, S. Olden, L. Lighty, J.L. Eastman, B. Doty, P. Dirmeyer, J. Adams, K. Mitchell, E. F. Wood and J. Sheffield, 2006: Land Information System - An Interoperable Framework for High Resolution Land Surface

Modeling. *Environmental Modelling & Software*, **21**, 1402-1415, doi:10.1016/j.envsoft.2005.07.004

Luo, A., Robock, K.Y. Vinnikov, C.A. Schlosser, A.G. Slater, N.A. Speranskaya, A. Boone, H. Braden, F. Chen, P. Cox, P. Rosnay, C.E. Desborough, R.E. Dickinson, Y.-J. Dai, Q. Duan, J. Entin, P. Etchevers, A. Henderson-Sellers, N. Gedney, Y.M. Gusev, F. Habets, J. Kim, V. Koren, E. Kowalczyk, K. Mitchell, O.N. Nasonova, J. Noilhan, A.J. Pitman, J. Schaake, A.B. Shmakin, T.G. Smirnova, D. Verseghy, P. Wetzel, Y. Xue, Z.-L. Yang, and Q. Zeng, 2003: Effects of frozen soil on soil temperature, spring infiltration, and runoff: Results from the PILPS 2(d) Experiment at Valdai, Russia. *J. Hydrometeor.* **4**, 334-351, http://dx.doi.org/10.1175/1525-7541(2003)4<334:EOFSOS>2.0.CO;2.

Petzold, R. E., 1977: An estimation technique for snow surface albedo, *Climatolog. Bull.*, **21**, 1-11, (http://www.cmosarchives.ca/CB/cb110101.pdf).

Robinson, D. A., and G. Kukla, 1985: Maximum surface albedo of seasonally snow-covered lands in the Northern Hemisphere, *J. Clim. Appl. Meteorol.*, **24**, 402–411, http://dx.doi.org/10.1175/1520-0450(1985)024<0402:MSAOSS>2.0.CO;2.

Robock, A., The seasonal cycle of snow cover, sea ice and surface albedo, 1980: *Mon. Wea. Review,* **108**, 267-285, http://dx.doi.org/10.1175/1520-0493(1980)108<0267:TSCOSC>2.0.CO;2.

Rutter, N, R Essery, J Pomeroy, N Altimir, K Andreadis, I Baker, A Barr, P Bartlett, A Boone, H Deng, H Douville, E Dutra, K Elder, C Ellis, X Feng, A Gelfan, A Goodbody, Y Gusev, D Gustafsson, R Hellstrom, Y Hirabayashi, T Hirota, T Jonas, V Koren, A Kuraqina, D Lettenmaier, W-P Li, C Luce, E Martin, O Nasonova, J Pumpanen, R Pyles, P Samuelsson, M Sandells, G Schaedler, A

Shmakin, T Smirnova, M Staehli, R Stoeckli, U Strasser, H Sua, K Suzuki, K Takata, K Tanaka, E Thompson, T Vesala, P Viterbo, A Wiltshire, K Xia, Y Xue and T Yamazaki, 2009: Evaluation of forest snow processes models (SnowMIP2). *Journal of Geophysical Research*, **114**, D06111, doi:10.1029/2008JD011063.

Schlosser, C. A., A. Robock, K. Y. Vinnikov, N. A. Speranskaya, and Y. Xue, 1997: 18-year land surface hydrology model simulations for a midlatitude grassland catchment in Valdai, Russia, *Mon. Weather Rev.,* **125***,* 3279–3296, http://dx.doi.org/10.1175/1520-0493(1997)125<3279:YLSHMS>2.0.CO;2.

Skamarock, W. C., J. B. Klemp, J. Dudhia, D. O. Gill, D. M. Barker, W. Wang and J. G. Powers, 2005, A Description of the Advanced Research WRF Version 2., http://www.mmm.ucar.edu/wrf/users/docs/arw_v2.pdf

Slater, A.G., C.A. Schlosser, C.E. Desborough, A.J. Pitman, A. Henderson-Sellers, A. Robock, K.Ya. Vinnikov, K. Mitchell, A. Boone, H. Braden, F. Chen, P.M. Cox, P. de Rosnay, R.E. Dickinson, Y.-J. Dai, Q. Duan, J. Entin, P. Etchevers, N. Gedney, Ye. M. Gusev, F. Habets, J. Kim, V. Koren, E.A. Kowalczyk, O.N. Nasonova, J. Noilhan, S. Schaake, A.B. Shmakin, T.G. Smirnova, D. Verseghy, P. Wetzel, Y. Xue, Z.-L. Yang, and Q. Zeng, 2001: The representation of snow in land surface schemes: Results from PILPS 2(d). *J. Hydrometeor.* **2**, 7-25, http://dx.doi.org/10.1175/1525-7541(2001)002<0007:TROSIL>2.0.CO;2.

Smirnova, T.G., J.M. Brown, and S.G. Benjamin, 1997: Performance of different soil model configurations in simulating ground surface temperature and surface fluxes. *Mon. Wea. Rev.* **125**, 1870-1884, http://dx.doi.org/10.1175/15200493(1997)125<1870:PODSMC>2.0.CO;2.

553 Smirnova, T.G., J.M. Brown, and D. Kim, 2000: Parameterization of cold-season processes in the MAPS
554 land-surface scheme. *J. Geophys. Res.* **105**, 4077-4086, doi: 10.1029/1999JD901047.

555 Smith, T. L., S. G. Benjamin, J. M. Brown, S. Weygandt, T. Smirnova, B. Schwartz, 2008: Convection
556 forecasts from the hourly updated, 3-km High Resolution Rapid Refresh (HRRR)
557 Model. Preprints, 24th Conf. on Severe Local Storms, Savannah, GA, Amer. Meteor. Soc.
558 (https://ams.confex.com/ams/pdfpapers/142055.pdf)

559 Tian, Y., Zhang, Y., Knyazikhin, J., Myneni, R.B., Glassy, J., Dedieu, G. and Running, S.W., 2000.
560 Prototyping of MODIS LAI and FPAR algorithm with LASUR and LANDSAT data. *IEEE Trans.*
561 *Geosci. Remote Sens.*, **38(5)**: 2387-2401,
562 (http://cybele.bu.edu/download/manuscripts/modisproto.pdf)

563 Thomas, G., and P. R. Rowntree, 1992: The boreal forests and climate, *Q. J. R. Meteorol. Soc.,* 118,
564 469–497, doi: 10.1002/qj.49711850505.

565 Viterbo, P., and A. K. Betts, 1999: Impact on ECMWF forecasts of changes to the albedo of the boreal
566 forests in the presence of snow, *J. Geophys. Res.,* **104**, 27803–27810, doi:
567 10.1029/1998JD200076.

568 Wang, W., C. Bruyere, M. Duda, J. Dudhia, D. Gill, M. Kavulich, K. Keene, H.-C. Lin, J. Michalakes, S.
569 Rizvi, X. Zhang, J. Berner and K. Smith, 2014: User's Guide for the Advanced Research WRF
570 (ARW) Modeling System Version 3.6.
571 http://www2.mmm.ucar.edu/wrf/users/docs/user_guide_V3/contents.html

572 Zubov N.N., 1963: Arctic Ice, Publisher: San Diego CA US Navy Electronics Laboratory, 510 pp.

RUC LSM characteristics	Version –Smirnova et al. 2000	Version – WRF version 3.6, 2014
Prognostic vertical levels	Soil - 6 levels (0, 5, 20, 40, 160, 300 cm) Snow – 2 levels	Soil – 9 levels (0, 1, 4, 10, 30, 60, 100, 160, 300 cm) Snow – 2 levels
Sea ice model	None	Simple treatment of sea ice/snow model
Snow model	2-layer snow model, snow area trimming	2-layer snow model with improvements in snow melting algorithm, snow area trimming/building
Snow melting	Single-iteration energy budget	Two-iteration energy budget
Snow albedo	Constant value – 0.75	Clear sky maximum surface albedo of snow-covered land computed from Defense Meteorological Satellite Program (DMSP) imagery, temperature dependence
Land-use classification	USGS categories	MODIS IGBP-modified categories
Vegetation fraction, Leaf area index (LAI)	0.144^{o}-resolution AVHRR vegetation fraction, no LAI	1-km resolution MODIS FPAR/LAI data;
Surface parameters	Look-up tables for dominant category	Sub-grid scale heterogeneity, includes seasonal variations

573

574 Table 1. Modifications to the RUC LSM implemented in the WRF version 3.6 model (2014) compared

575 to its predecessor 2000 version. Abbreviations: MODIS (Moderate-Resolution Imaging

576 Spectroradiometer), FPAR (Fractional Photosynthetically Active Radiation), IGBP (International

577 Geosphere-Biosphere Programme), AVHRR (Advanced Very High Resolution Radiometer)

578

Figure Captions.

Figure 1. Topography image (elevation in meters) of the North America RAP domain with embedded RUC domain also shown (assumed to be equal to the conterminous US (CONUS) in this paper).

Figure 2. 2-m temperature bias (forecast minus observations) from the RAP 12-h forecasts using 6-level (red) and 9-level (blue) versions of the RUC LSM over entire RUC domain (Fig. 1).

Figure 3. Comparison of Rapid Refresh 12-hour forecasts, valid at 00 UTC 14 May 2009, of (a) skin temperature, (b) sensible heat flux, and (c) flux into snow/sea ice in the Arctic region of RAP . Left images are for the RUC LSM without sea-ice parameterization and images on the right are with the sea-ice parameterization.

Figure 4. (a) RAP 12-hour forecast over Alaska for 850 hPa temperature (C), height (m) and wind (knots), and (b) and (c) 2-m temperature errors (C, forecast minus observation) with (b) old and (c) new treatment of sea ice. Circled regions are affected by the airmass formed over sea ice. Valid time 1200 UTC 30 March 2009.

Figure 5. RAP forecast error vs. METAR surface observations. (a) – biases (forecast minus observations) and (b) – RMS errors for 12-hour forecasts of 2-m temperature averaged over CONUS domain (Fig. 1) for 1-10 January 2015. Control run (red line) – uses old snow melting algorithm; test run (blue line) – utilizes two-iteration snow melting approach

Figure 6. Cycled RAP snow depth over CONUS domain valid at 0600 UTC on 4 January 2015 from (a) the control run with old snow melting algorithm, and (b) the test run with the two-iteration snow melting approach. (c) Snow depth from the NOHRSC (National Operational Hydrologic Remote Sensing Center) Snow Analyses valid at 0600 UTC 4 January 2015. Red oval indicates the area with improved snow cover from the new snow melting approach.

Figure 7. Maximum surface albedo of snow-covered land measured from Defense Meteorological Satellite Program (DMSP) imagery in 1 x 1° latitude-longtitude cells (Robinson and Kukla, 1985) for the 13-km RAP domain.

612 Figure 8. RAP 6-h forecast error of 2-m temperature vs. METAR surface observations. (a) – biases
613 (forecast minus observations) and (b) – STD errors averaged over eastern part of CONUS domain (Fig.
614 1) for 1-10 January 2015. Control run (red line) – uses constant value of fresh snow albedo equal to
615 0.75; test run (blue line) – utilizes clear-sky maximum surface albedo of snow-covered land,
616 computed from Defense Meteorological Satellite Program (DMSP) imagery brightness in 1° latitude–
617 longtitude cells (Robinson and Kukla, 1985); test minus control (black line).
618
619 Figure 9. Snow water equivalent during the winter season of 2003-2004 at a grassland location in
620 Alptal, Switzerland (47° N, 8° E, elevation 1220 m) (data provided by Swiss Federal Institute for Forest,
621 Snow and Landscape Research WSL): (a) – simulation from all 27 models participating in SnowMIP2
622 experiment (red – average over 27 models, green dots – observed); (b) – snow water equivalent
623 observed (blue triangles), and from RUC LSM with the constant snow albedo equal to 0.75 (red curve)
624 and with albedo dependent on surface temperature (green curve).
625
626 Figure 10. Snow/ice albedo in the Arctic region of Rapid Refresh domain (Lambert conformal
627 projection) for 13 May 2009: (a) – before implementation of snow/ice albedo temperature
628 dependence; (b) – after implementation of snow/ice albedo temperature dependence.
629
630 Figure 11. USGS dominant land-use categories for Rapid Refresh domain.
631
632 Figure 12. MODIS dominant land-use categories for Rapid Refresh domain.
633

Figure 13. Roughness length specified from USGS land-use classification minus roughness length from MODIS classification (a) – with the use of dominant category approach and (b) – with subgrid heterogeneity taken into account.

Figure 14. RAP 10-m wind speed bias vs. METAR observations for 12-hour forecasts averaged over entire RUC domain (Fig. 1) for 16-25 May 2013. Control run – utilizes dominant category approach (in red), test run – takes into account subgrid heterogeneity (in blue); test minus control (in black).

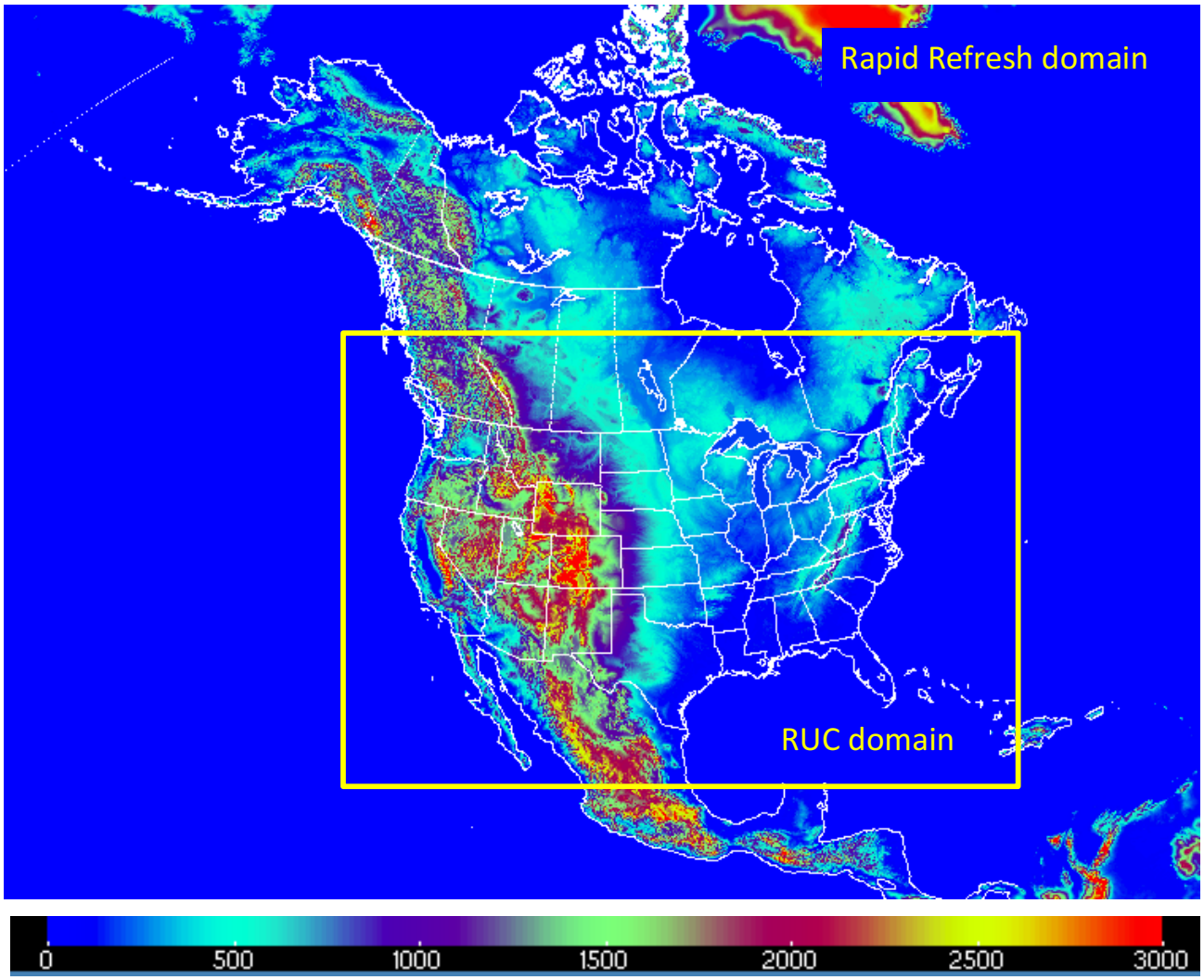

Figure 1. Topography image (elevation in meters) of the North America RAP domain with embedded RUC domain also shown (assumed to be equal to the conterminous US (CONUS) in this paper).

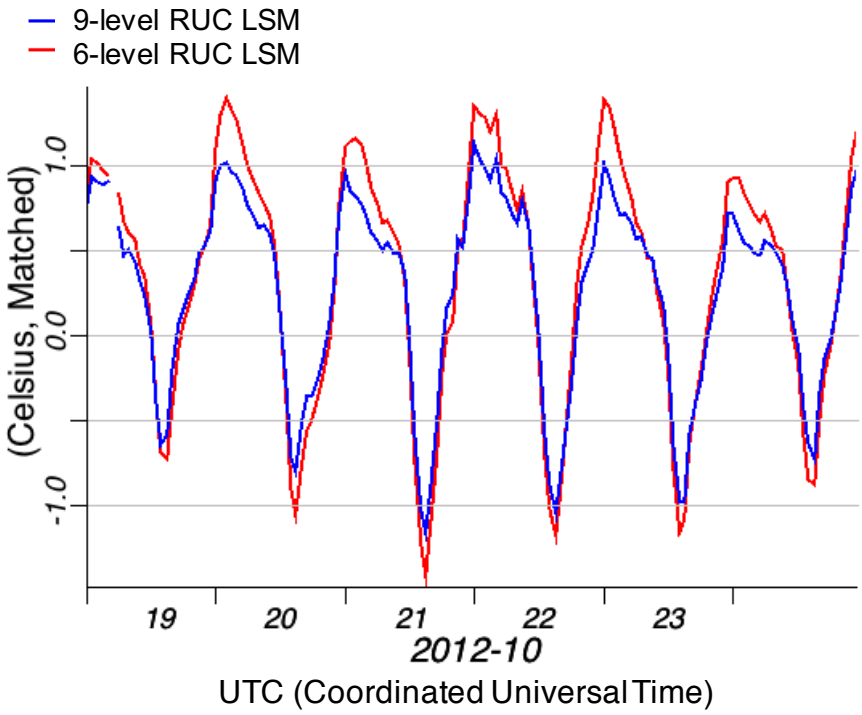

645

646

647 Figure 2. 2-m temperature bias (forecast minus observations) from the RAP 12-h forecasts using 6-

648 level (red) and 9-level (blue) versions of the RUC LSM over entire RUC domain (Fig. 1).

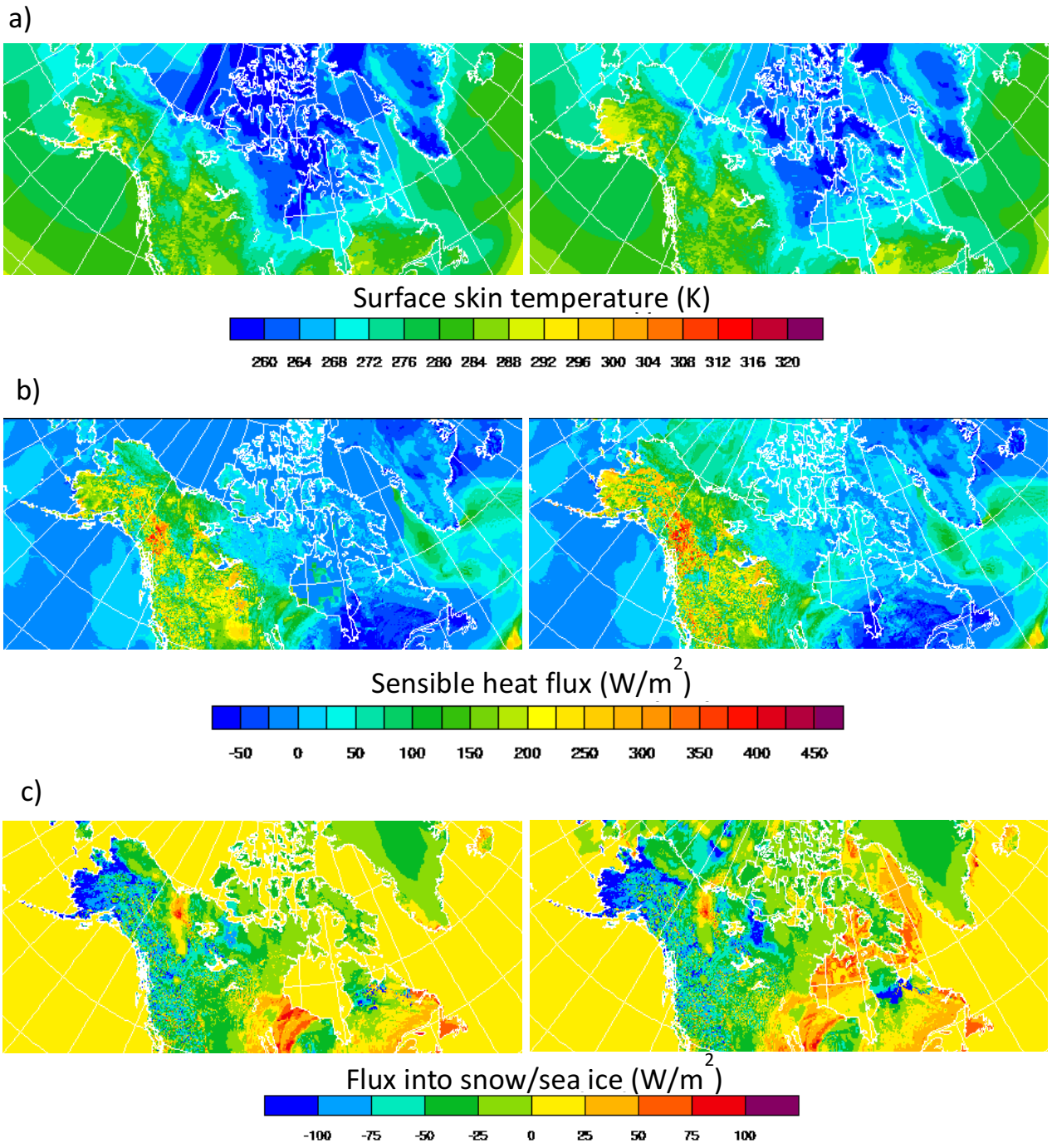

Figure 3. Comparison of Rapid Refresh 12-hour forecasts, valid at 00 UTC 14 May 2009, of (a) skin temperature, (b) sensible heat flux, and (c) flux into snow/sea ice in the Arctic region of RAP . Left images are for the RUC LSM without sea-ice parameterization and images on the right are with the sea-ice parameterization.

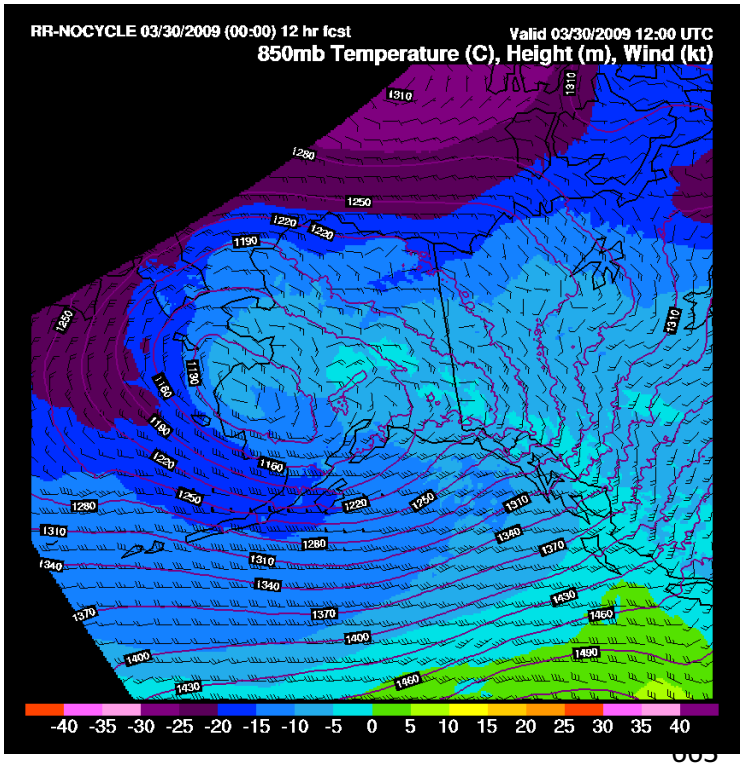

a)

b)

c)

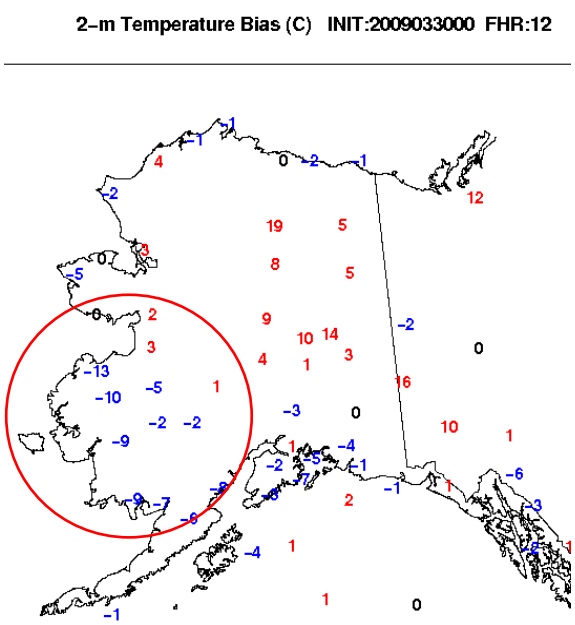

Old approach

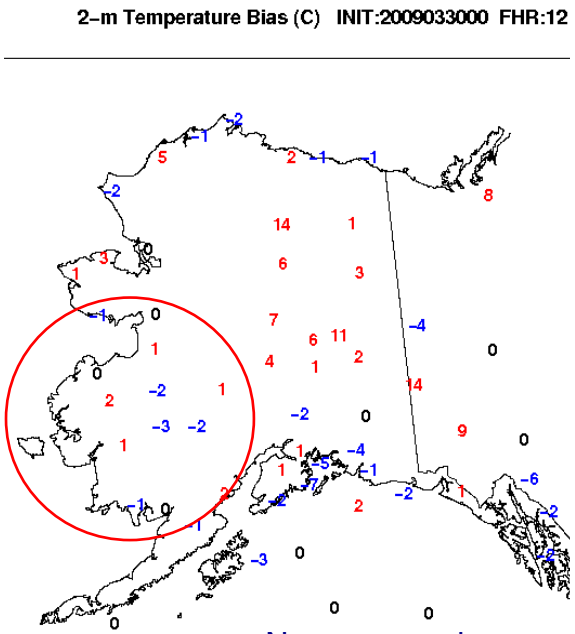

New approach

666

667 Figure 4. (a) RAP 12-hour forecast over Alaska for 850 hPa temperature (C), height (m) and
668 wind (knots), and (b) and (c) 2-m temperature errors (C, forecast minus observation) with (b)
669 old and (c) new treatment of sea ice. Circled regions are affected by the airmass formed over
670 sea ice. Valid time 1200 UTC 30 March 2009.

671

a) b)

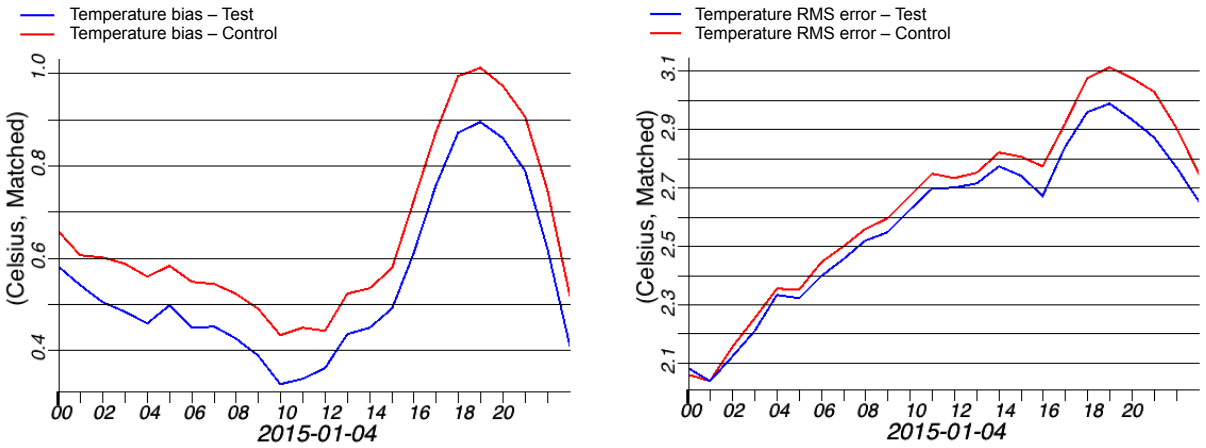

672

673 Figure 5. RAP forecast error vs. METAR surface observations. (a) – biases (forecast minus

674 observations) and (b) – RMS errors for 12-hour forecasts of 2-m temperature averaged over

675 CONUS domain (Fig. 1) for 1-10 January 2015. Control run (red line) – uses old snow melting

676 algorithm; test run (blue line) – utilizes two-iteration snow melting approach.

677

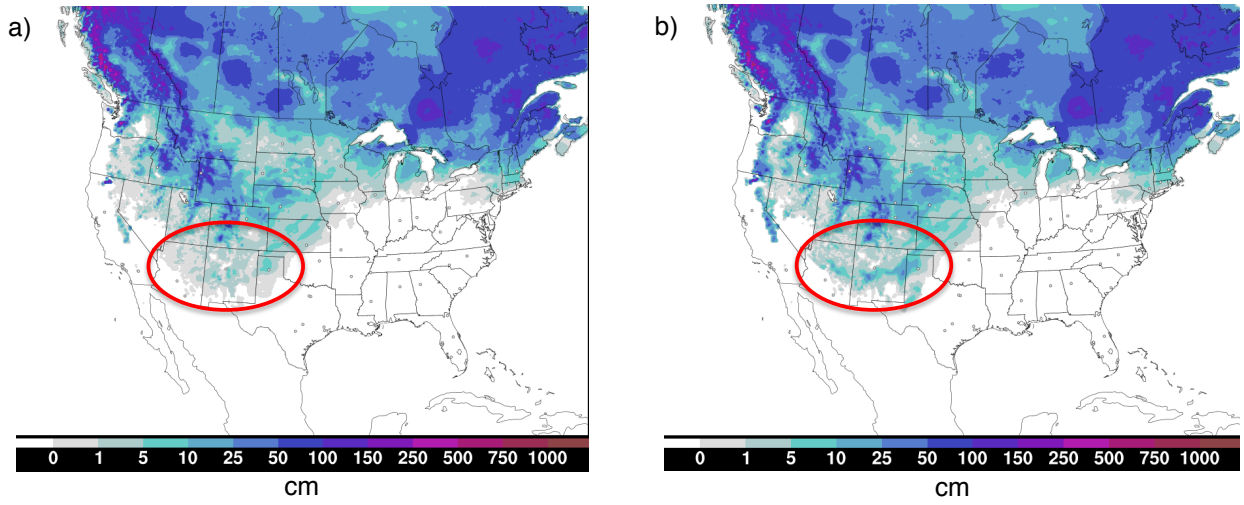

678

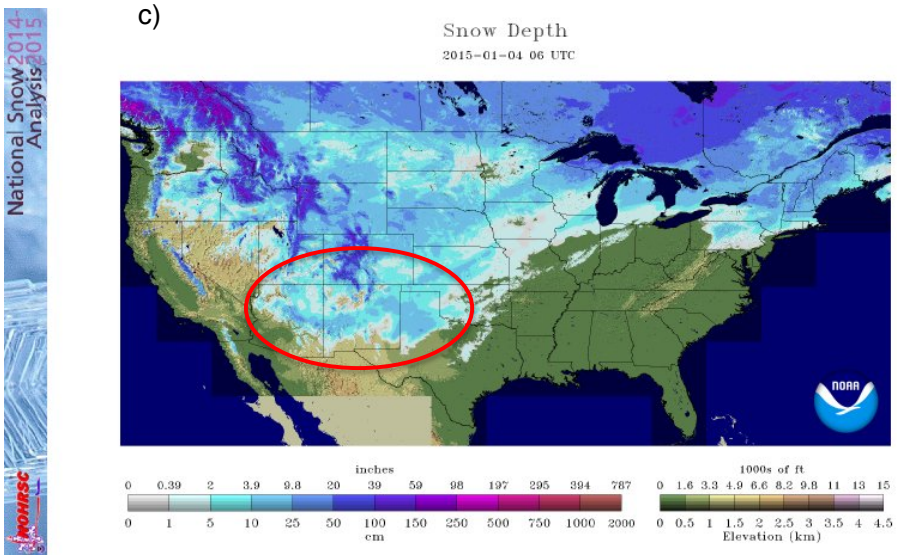

679

680 Figure 6. Cycled RAP snow depth over CONUS domain valid at 0600 UTC on 4 January 2015 from
681 (a) the control run with old snow melting algorithm, and (b) the test run with the two-iteration
682 snow melting approach. (c) Snow depth from the NOHRSC (National Operational Hydrologic
683 Remote Sensing Center) Snow Analyses valid at 0600 UTC 4 January 2015. Red oval indicates
684 the area with improved snow cover from the new snow melting approach.

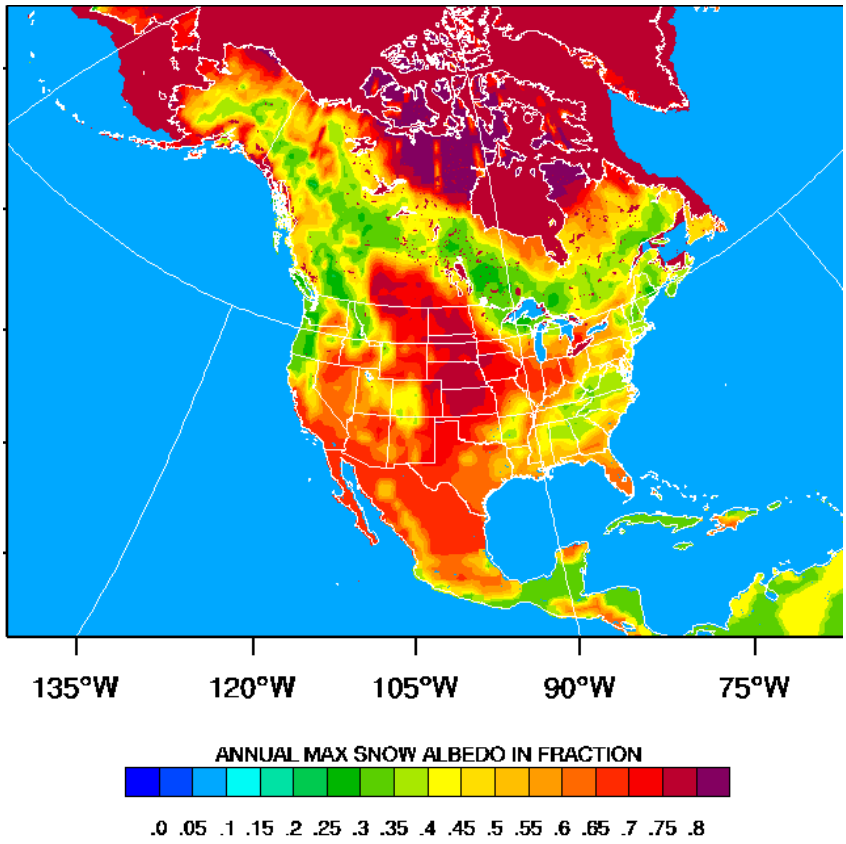

685

686 Figure 7. Maximum surface albedo of snow-covered land measured from Defense

687 Meteorological Satellite Program (DMSP) imagery in 1 x 1° latitude-longtitude cells (Robinson

688 and Kukla, 1985) for the 13-km RAP domain.

a)

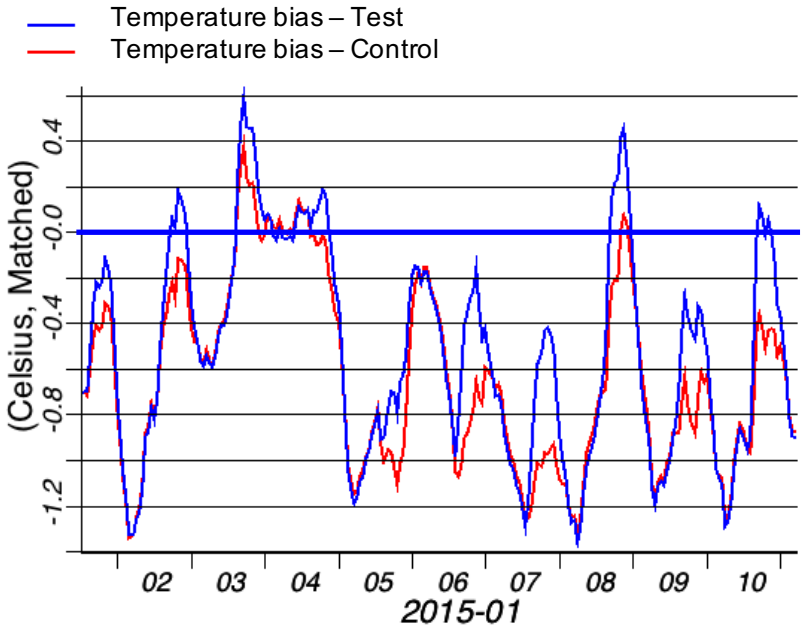

UTC (Coordinated Universal Time)

689

b)

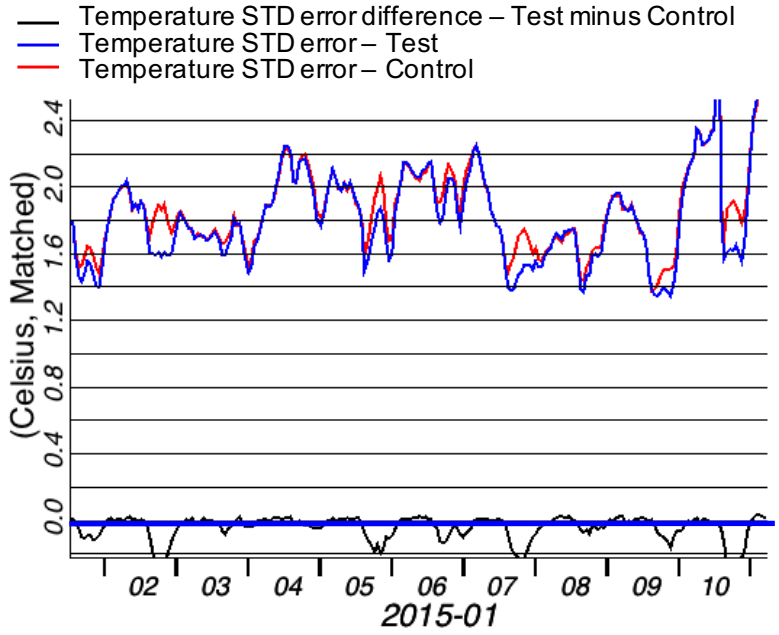

UTC (Coordinated Universal Time)

690

691 Figure 8 RAP 6-h forecast error of 2-m temperature vs. METAR surface observations. (a) –
692 biases (forecast minus observations) and (b) – STD errors averaged over eastern part of CONUS
693 domain (Fig. 1) for 1-10 January 2015. Control run (red line) – uses constant value of fresh
694 snow albedo equal to 0.75; test run (blue line) – utilizes clear-sky maximum surface albedo of
695 snow-covered land, computed from Defense Meteorological Satellite Program (DMSP) imagery
696 brightness in 1° latitude–longtitude cells (Robinson and Kukla, 1985); test minus control (black
697 line).

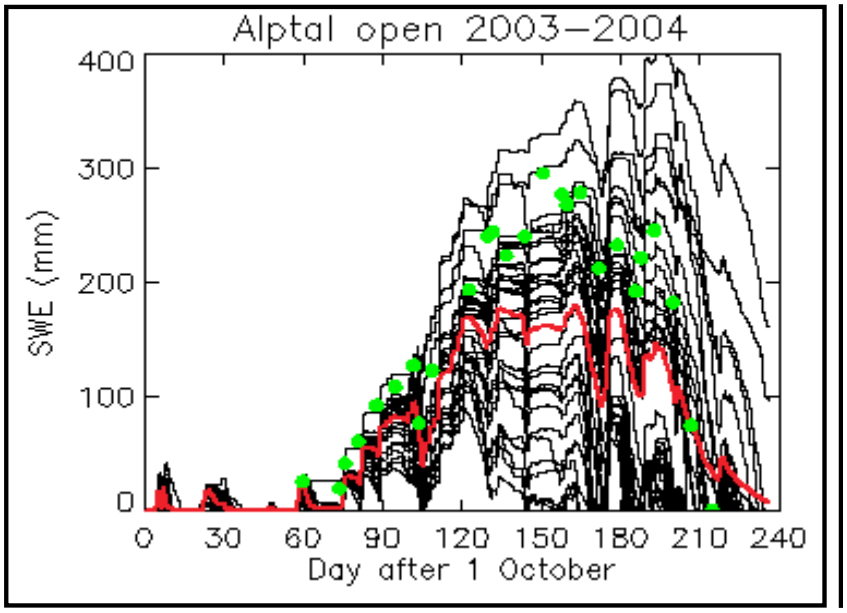

a)

705

b)

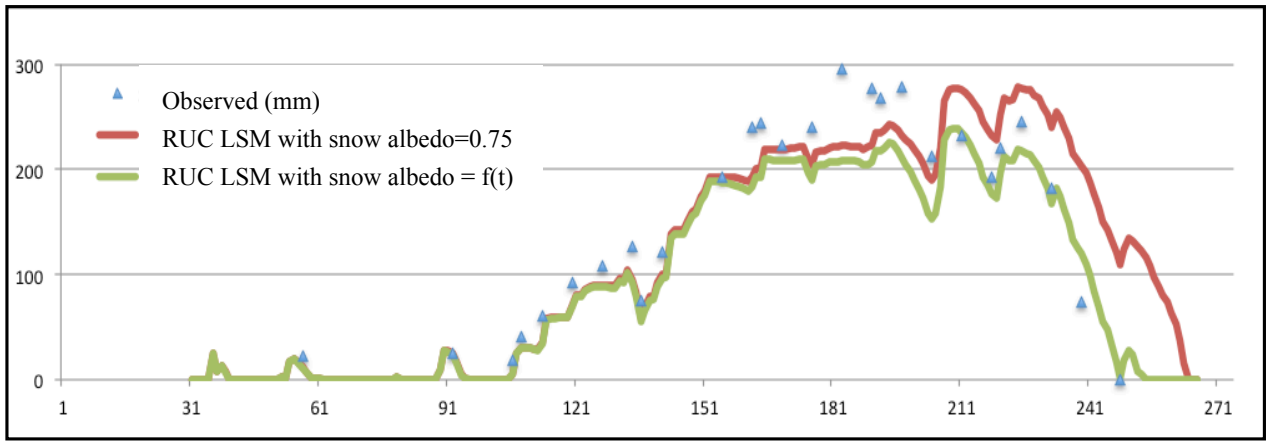

706

707 Figure 9. Snow water equivalent during the winter season of 2003-2004 at a grassland location
708 in Alptal, Switzerland (47° N, 8° E, elevation 1220 m) (data provided by Swiss Federal Institute
709 for Forest, Snow and Landscape Research WSL): (a) – simulation from all 27 models
710 participating in SnowMIP2 experiment (red – average over 27 models, green dots – observed);
711 (b) – snow water equivalent observed (blue triangles), and from RUC LSM with the constant

712 snow albedo equal to 0.75 (red curve) and with albedo dependent on surface temperature

713 (green curve).

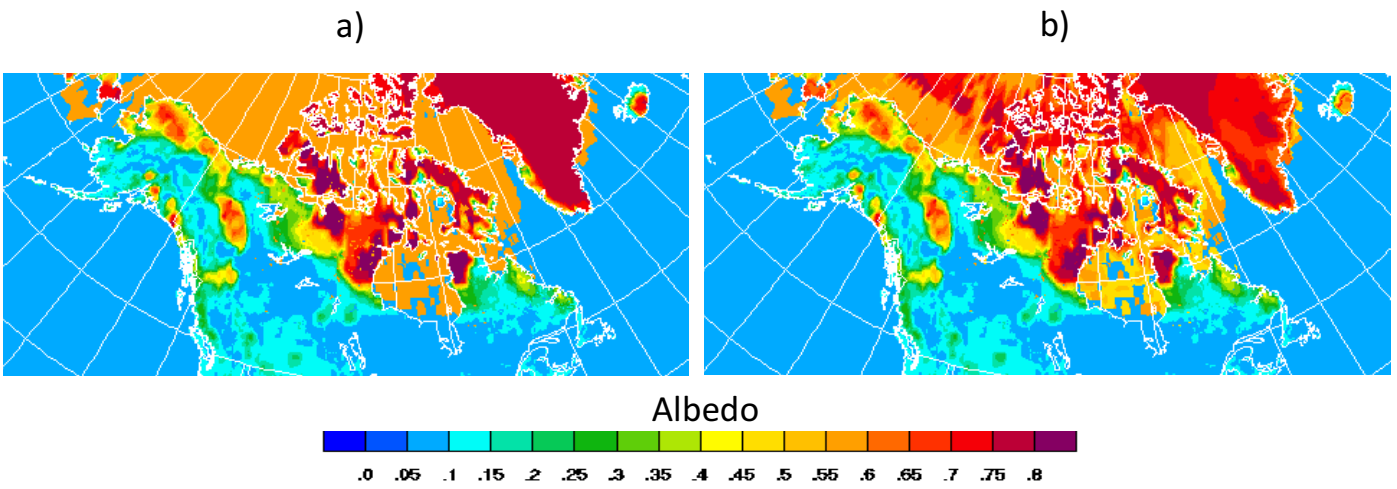

714

715 Figure 10. Snow/ice albedo in the Arctic region of Rapid Refresh domain (Lambert conformal

716 projection) for 13 May 2009: (a) – before implementation of snow/ice albedo temperature

717 dependence; (b) – after implementation of snow/ice albedo temperature dependence.

718

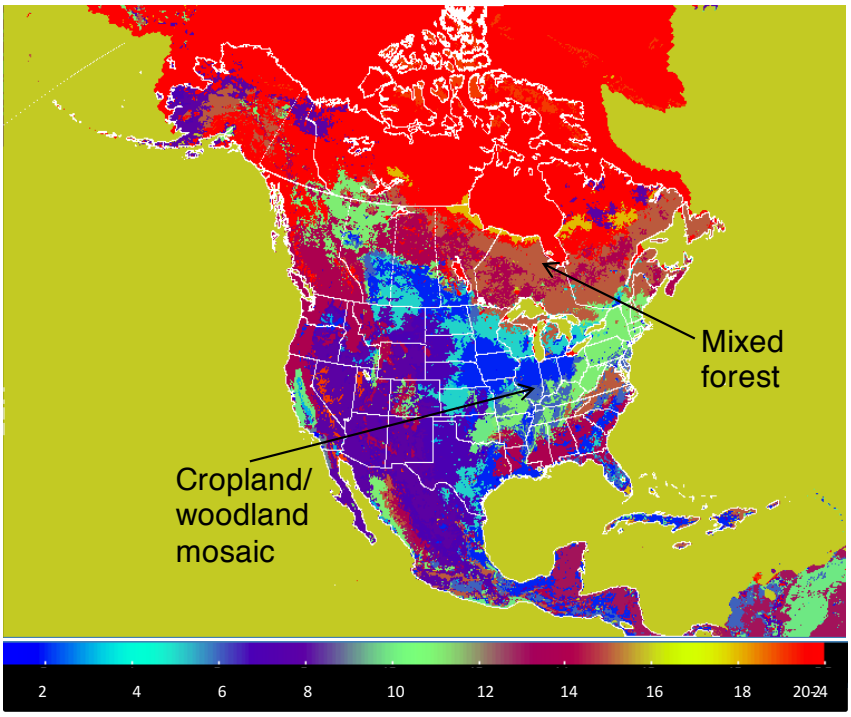

1. Urban and Built-Up Land
2. Dryland Cropland and Pasture
3. Irrigated Cropland and Pasture
4. Mixed Dryland/Irrigated Cropland and Pasture
5. Cropland/Grassland Mosaic
6. Cropland/Woodland Mosaic
7. Grassland
8. Shrubland
9. Mixed Shrubland/Grassland
10. Savanna
11. Deciduous Broadleaf Forest
12. Deciduous Needleleaf Forest
13. Evergreen Broadleaf Forest
14. Evergreen Needleleaf Forest
15. Mixed Forest
16. Water
17. Herbaceous Wetland
18. Wooded Wetland
19. Barren or Sparsely Vegetated
20. Herbaceous Tundra
21. Wooded Tundra
22. Mixed Tundra
23. Bare Ground Tundra
24. Snow or Ice (valid time – 9 January 2015)

719

720 Figure 11. USGS dominant land-use categories for Rapid Refresh domain.

721

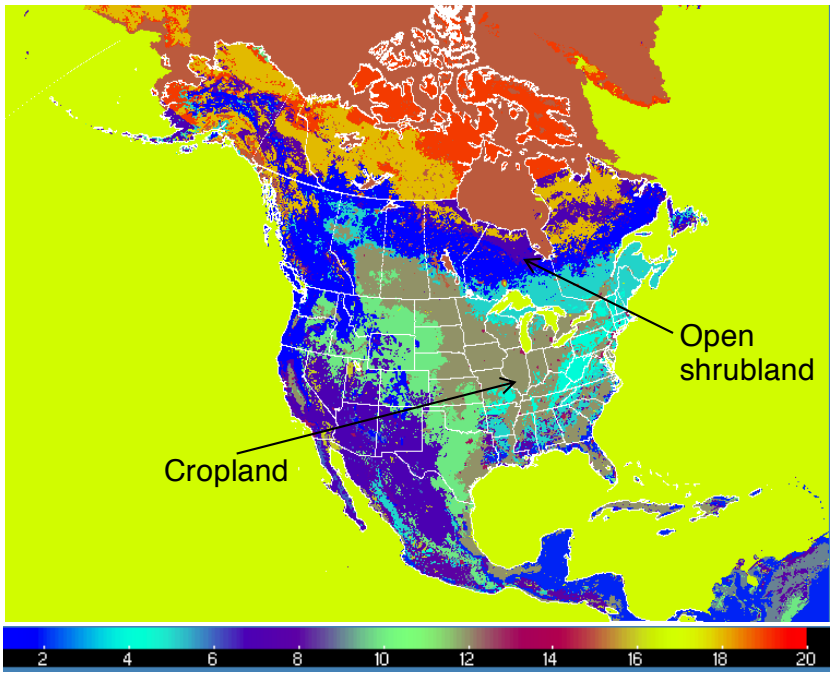

1. Evergreen Needleleaf Forest
2. Evergreen Broadleaf Forest
3. Deciduous Needleleaf Forest
4. Deciduous Broadleaf Forest
5. Mixed Forests
6. Closed Shrublands
7. Open Shrublands
8. Woody Savannas
9. Savannas
10. Grasslands
11. Permanent wetlands
12. Croplands
13. Urban and Built-Up
14. Cropland/natural vegetation mosaic
15. Snow and Ice (valid time – 9 January 2015)
16. Barren or Sparsely Vegetated
17. Water
18. Wooded Tundra
19. Mixed Tundra
20. Barren Tundra

722

723 Figure 12. MODIS dominant land-use categories for Rapid Refresh domain.

724

a)

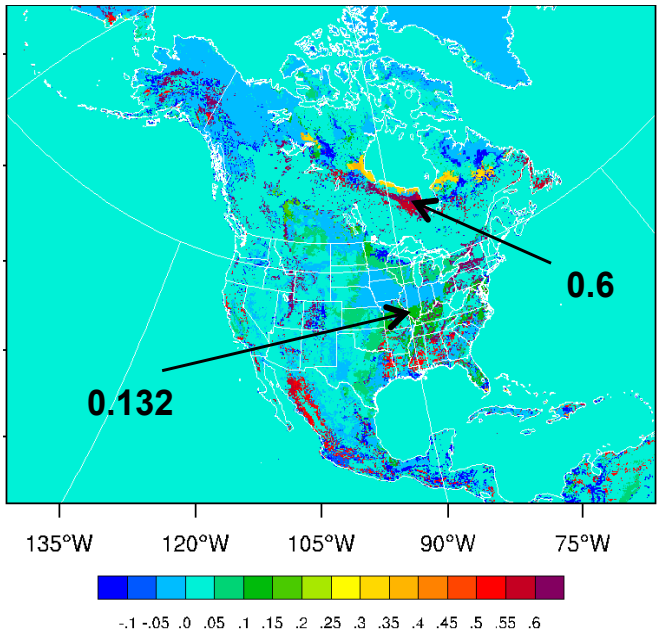

725

b)

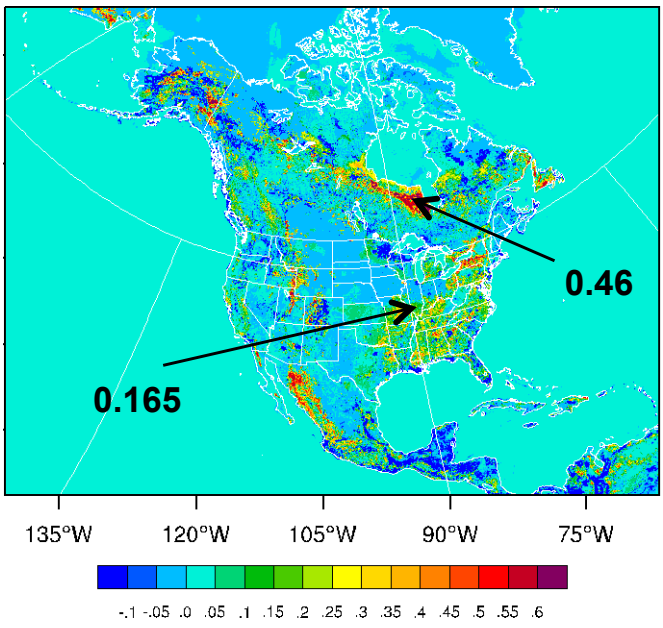

726

727 Figure 13. Roughness length specified from USGS land-use classification minus roughness length

728 from MODIS classification. (a) – with the use of dominant category approach and (b) – with

729 subgrid heterogeneity taken into account.

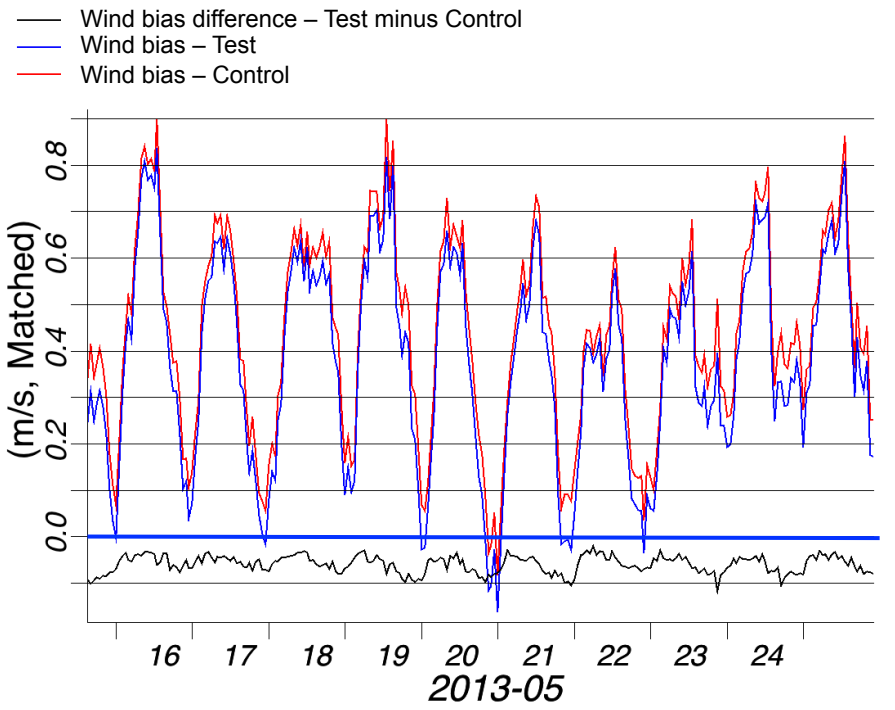

730

731 Figure 14. RAP 10-m wind speed bias vs. METAR observations for 12-hour forecasts averaged

732 over entire RUC domain (Fig. 1) for 16-25 May 2013. Control run – utilizes dominant category

733 approach (in red), test run – takes into account subgrid heterogeneity (in blue); test minus

734 control (in black).